

# Effects of doping on spin correlations in the periodic Anderson model

J. Bonča

*Department of Physics, FMF, University of Ljubljana and J. Stefan Institute, Ljubljana, Slovenia*

J. E. Gubernatis

*Theoretical Division, Los Alamos National Laboratory, Los Alamos, NM 87545*

(February 24, 2018)

## Abstract

We studied the effects of hole doping on spin correlations in the periodic Anderson model, mainly at the full and three-quarters-full lower bands cases. In the full lower band case, strong anti-ferromagnetic correlations develop when the on-site repulsive interaction strength  $U$  becomes comparable to the quasi-particle band width. In the three-quarters full case, a novel kind of spin correlation develops that is consistent with the resonance between a  $(\pi, 0)$  and a  $(0, \pi)$  spin-density wave. In this state the spins on different sublattices appear uncorrelated. Hole doping away from the completely full case rapidly destroys the long-range anti-ferromagnetic correlations, in a manner reminiscent of the destruction of anti-ferromagnetism in the Hubbard model. In contrast to the Hubbard model, the doping does not shift the peak in the magnetic structure factor from the  $(\pi, \pi)$  position. At dopings intermediate to the full and three-quarters full cases, only weak spin correlations exist.

Typeset using REVTeX

## I. INTRODUCTION

We report the results of a quantum Monte Carlo study on the effects of hole doping on spin correlations in the two-dimensional asymmetric periodic Anderson model. Our undoped state is the insulating state which exists when the lower band is full. When the on-site Coulomb repulsion is sufficiently large, this state is also anti-ferromagnetic. On the one hand, we will argue that the effects of hole doping on this state are similar to those found in doping studies of the Hubbard model's half-filled state as we find that the doping rapidly destroys the anti-ferromagnetism. On the other hand, we will argue that continued doping to a 3/4-filling of the lower band produces a novel ground-state, not reported for the Hubbard model, that we interpret as a state resonating between two spin-density wave states. In this state, spins on the different sub-lattices of the bipartite square lattice are uncorrelated.

Fewer analytic studies exist for the periodic Anderson model (PAM) than for the Hubbard model. Yet the published literature is still vast. In one, two, three, and infinite dimensions for strong and weak coupling limits of the interaction strengths, many different investigators have studied this model by using conserving approximations, the density-matrix renormalization group method, the Hartree-Fock, slave boson, and dynamical mean-field approximations, the exact diagonalization method, and various variational methods. If studied, the effect of doping was found to induce paramagnetic, ferromagnetic, anti-ferromagnetic, and spiral spin states at various temperatures and interaction strengths. Interest in the periodic Anderson model has traditionally been driven by interests in mixed valent, heavy fermion, and Kondo insulating materials. Possible application to these classes of materials motivated the present study.

Far fewer quantum Monte Carlo (QMC) studies exist for the Anderson model than for the Hubbard model. Most have been for the one-dimensional symmetric PAM. In fact we are aware of only 2 one-dimensional studies of the asymmetric PAM<sup>1</sup> and 2 two-dimensional simulations<sup>2,3</sup> of the symmetric PAM. Both two-dimensional studies were simulations at low

but finite temperature and focused on the symmetric PAM at half-filling to avoid the Fermion sign problem which produces exponentially growing variances in measured properties as the temperature is lowered, the lattice size is increased, and particle-hole symmetry is destroyed by doping.

Zhang and Callaway,<sup>2</sup> in the earlier paper of the two, concluded that the properties of the half-filled symmetric PAM had some qualitative similarities to those of the single-impurity Anderson model but at low temperatures some additional physics developed. In the single-impurity model, the electrons on the impurity site become correlated with the conduction electrons as the temperature is lowered to the Kondo temperature  $T_K$ . At temperatures much lower than  $T_K$ , the local moment on the impurity is spin compensated by the conduction electrons, leading to a non-magnetic state. Zhang and Callaway observed similar behavior in the lattice model. Short range correlations between the conduction electrons and the electrons localized on the f-orbitals screened these moments, and at very low temperatures these local moments became correlated through their interaction with the conduction electrons. The build-up of these correlations was seen in the behavior of the magnetic structure factor and the uniform magnetic susceptibilities. It is the development of the anti-ferromagnetic correlations among the f-orbitals that is the new physics in the periodic Anderson lattice model.<sup>4</sup>

More recently, Vekić et al.<sup>3</sup> found for the same model the same behavior observed by Zhang and Callaway, plus more as they explicitly sought to examine the competition between the tendency to anti-ferromagnetic order and to spin disorder. As noted by Doniach,<sup>5</sup> this competition is between the Ruderman-Kittel-Kasuya-Yosida (RKKY) interaction trying to order the f-moments and the Kondo interaction trying to screen them away. The Kondo interaction scales as  $T_K \sim W e^{-W/J}$ , and the RKKY interaction, as  $J_{RKKY} \sim J^2/W$ . ( $W$  is some band width, and  $J$  is the strength of the anti-ferromagnetic Kondo exchange interaction between the conduction band and f-electrons.) When  $J_{RKKY} > T_K$ , an anti-ferromagnetically ordered singlet ground state is expected. This will occur as long as  $J$  is less than a critical value  $J_c$ . When  $J > J_c$  a Kondo spin-compensated ground state

is expected. For the PAM,  $J \sim V^2/U$ , where  $V$  is the strength of the hybridization between the f-electrons and the conduction band electrons and  $U$  is the value of the repulsive on-site Coulomb interaction. Consequently, when  $U$  is large,  $J$  is small, and an anti-ferromagnetically ordered state is expected. As the value of  $U$  is lowered, a cross-over to a disordered ground-state eventually occurs. The general conclusions of Vekić et al. are even broader: For small values  $J$ , the ground state of the PAM is an insulator with long-range anti-ferromagnetic order characterized by a finite charge gap and gapless spin excitations. As  $J$  increases, the long-range order is destroyed, and the system exhibits spin-liquid behavior, which is a disordered spin state with both a spin and charge gap. When  $J1 <$  is sufficiently large, the system crosses over to a band-insulating state, and the size of the spin and charge gaps approach each other.

In this report we used a new ground-state QMC method, the constrained-path Monte Carlo method (CPMC), to study the properties of the asymmetric two-dimensional PAM. This method<sup>6</sup> eliminates the Fermion sign problem that plagues most QMC methods for simulating systems of interacting electrons. It accomplishes this by imposing an approximate condition constraining the random walk of the ground state wavefunction. Testing and comparing with other simulations has demonstrated<sup>6-9</sup> that the estimated energy and the predicted correlation functions are very accurate. Consequently, with this method we can more effectively study doped systems than we could with other QMC methods.<sup>10</sup>

We limited our numerical study of the PAM to select ranges of interaction strengths and dopings. In the undoped state, we positioned the energy of the f-orbital into the lower band and increased the strength of the on-site Coulomb interaction until on the average one electron occupied each f-orbital with a nearly saturated magnetic moment. From the work of Vekić et al., we expect a gap in the density of states and long-range anti-ferromagnetic order among the moments on the f-orbitals. Hole doping changes the nature of the indirect exchange interaction and thus the nature of the spin correlations. For the PAM, doping also rapidly destroys the anti-ferromagnetic state, and sufficient doping produces a novel state which we call the resonating spin-density-wave (RSDW) state. Our main purpose is

to illustrate these results.

In the next Section we describe the PAM, emphasizing its features when the on-site interaction strength  $U$  is zero. These features suggest the possibility of a magnetic instability of the non-interacting electron gas at several electron densities. Then in Section III, we give a qualitative description of the CPMC method. Details have been reported elsewhere.<sup>6</sup> In Section IV, we present our numerical results. We emphasize the wavenumber dependence of the electron density and the spin-spin correlation function. Lastly, in Section V, we present summarizing remarks and suggestions for future work.

## II. PERIODIC ANDERSON MODEL

For the Hamiltonian describing the PAM we took

$$\begin{aligned}
 H = & -t \sum_{\langle i,j \rangle, \sigma} (d_{i,\sigma}^\dagger d_{j,\sigma} + d_{j,\sigma}^\dagger d_{i,\sigma}) + V \sum_{i,\sigma} (d_{i,\sigma}^\dagger f_{i,\sigma} + f_{i,\sigma}^\dagger d_{i,\sigma}) \\
 & + \epsilon_f \sum_{i,\sigma} n_{i,\sigma}^f + \frac{1}{2} U \sum_{i,\sigma} n_{i,\sigma}^f n_{i,-\sigma}^f
 \end{aligned} \tag{1}$$

where the creation and destruction operators create and destroy d-electrons on sites of a square lattice and f-electrons on orbitals associated with these sites.  $n_{i,\sigma}^f = f_{i,\sigma}^\dagger f_{i,\sigma}$  is the number operator for f-electrons. Elsewhere we will use a similar notation to denote quantities like  $n_{i,\sigma}^d = d_{i,\sigma}^\dagger d_{i,\sigma}$ , the number operator for d electrons. The lattice has  $N$  sites, and hopping only occurs between neighboring lattice sites and between a lattice site and its orbital. We used periodic boundary conditions and took  $t = 1$ .

From (1) we define  $H_{00}$  and  $H_0$ , the resulting Hamiltonians when  $V = U = 0$  and  $U = 0$ .  $H_{00}$  has two energy bands, each holding up to  $N$  electrons of each spin  $\sigma$ . One band is dispersionless with a value of  $\epsilon_f$ . The other is dispersive with  $2N$  states labeled by the wavevector  $\mathbf{k} = (k_x, k_y)$  and spin  $\sigma$  and is given by

$$e_\sigma(\mathbf{k}) = -2[\cos(k_x) + \cos(k_y)] \tag{2}$$

Thus for  $N$  lattice sites there are  $4N$  available energy states. A half-filled system corresponds to  $2N$  electrons.

$H_0$  has two dispersive bands

$$E_{\sigma}^{\pm}(\mathbf{k}) = \frac{1}{2} \left[ e_{\sigma}(\mathbf{k}) + \epsilon_f \pm \sqrt{(e_{\sigma}(\mathbf{k}) - \epsilon_f)^2 + 4V^2} \right] \quad (3)$$

separated by a gap

$$\Delta = E_{\sigma}^{+}(0,0) - E_{\sigma}^{-}(\pi,\pi) = -4 + \frac{1}{2} \left[ \sqrt{(4 + \epsilon_f)^2 + 4V^2} + \sqrt{(4 - \epsilon_f)^2 + 4V^2} \right] \quad (4)$$

The operators which create quasi-particles in the lower and upper bands are of the form

$$\begin{aligned} \alpha_{\mathbf{k},\sigma}^{\dagger} &= \sum_i \left( Y_{\mathbf{k}i} f_{i,\sigma}^{\dagger} + X_{\mathbf{k}i} d_{i,\sigma}^{\dagger} \right) \\ \beta_{\mathbf{k},\sigma}^{\dagger} &= \sum_i \left( X_{\mathbf{k}i} f_{i,\sigma}^{\dagger} - Y_{\mathbf{k}i} d_{i,\sigma}^{\dagger} \right) \end{aligned} \quad (5)$$

and depending on the relative magnitudes of the matrices  $X$  and  $Y$ , a band can be f-like or d-like. If one band is f-like, then the other must be d-like. At half-filling, only the states in the lower band are filled. When this band itself is only half or more filled, it shows little dispersion among the states near the Fermi surface  $\mathbf{k}_F$ , meaning there is a large density of states at  $\mathbf{k}_F$  and the nearby band states are f-like. By contrast, the upper-band resembles the tight-binding band  $e_{\sigma}(\mathbf{k})$  and is thus d-like. The Brillouin zone for the square lattice is shown in Fig. 1. A plot of both bands and the tight-binding band along directions between high symmetry points in this zone is shown in Fig. 2. The tight-binding band was shifted so it and  $E_{+}(\mathbf{k})$  are equal at  $(\pi, \pi)$ .

All our simulations were done for hole dopings to less than half-filling. In the non-interacting case half-filling corresponds to a full lower band. *Because the way we dope, we found it more convenient, from this point on, to characterize our results in terms of the fractional filling of the lower band.* Also because of the way we dope, the properties of the lower band are obviously particularly important. The lower (valance) band has a width of

$$W = E_{\sigma}^{-}(\pi,\pi) - E_{\sigma}^{-}(0,0) = 4 - \frac{1}{2} \left[ \sqrt{(4 + \epsilon_f)^2 + 4V^2} - \sqrt{(4 - \epsilon_f)^2 + 4V^2} \right] \quad (6)$$

We only considered  $\epsilon_f = -2$  and  $V = 0.5$ , and for these values,  $\Delta = 0.16$  and  $W = 2.08$ . Thus we have a narrow band, with an enhanced density of states near the Fermi surface,

into which we will place the electrons and then induce strong correlations by adding strong repulsive Coulomb interactions. We also considered only a  $6 \times 6$  lattice size. In terms of computational effort this size is roughly equivalent to simulating a  $12 \times 12$  Hubbard model.

Often the symmetric version of the PAM is studied. In this case,  $\epsilon_f = -\frac{1}{2}U$  and at half-filling particle-hole symmetry exists. As  $U$  is varied so is the band-structure of the non-interacting problem. We chose to keep that structure fixed and vary the interaction strength. Over the range of parameters used, the dominance of  $T_K$  is replaced by  $J_{RKKY}$  as  $U$  is increased from 0. Accordingly, the ground-state is expected to go from a spin disordered to anti-ferromagnetically ordered one.<sup>3</sup>

The ground state of  $H_0$  does not show long-ranged spatial spin correlations, but at certain electron fillings the Fermi surface may be unstable towards the development of a spin-density wave when  $U \neq 0$ . Such instabilities arise if the nesting conditions,  $E_\sigma^-(\mathbf{k}) = E_\sigma^-(\mathbf{k}' + \mathbf{Q}) = E_\sigma^-(\mathbf{k}_F) \equiv E_F$  and  $E_\sigma^-(\mathbf{k}') = E_F$ , are satisfied.<sup>11</sup> For a commensurate state,  $\mathbf{Q}$  is a high symmetry point on the boundary of the Brillouin zone and equals one-half of a reciprocal lattice vector. For a square lattice there are two such points,  $(0, \pi)$  and  $(\pi, \pi)$ , and the nesting conditions lead to the set of thick lines in the Brillouin zone shown in Fig. 3. If portions of the Fermi surface approximate these lines, an instability of the Fermi surface is possible. (For the lower band, the critical fillings are  $\frac{1}{4}$ ,  $\frac{1}{2}$ , and  $\frac{3}{4}$ . In Fig. 3, we only show the nesting conditions relative to  $\frac{1}{2}$ , and  $\frac{3}{4}$  fillings.) In the  $6 \times 6$  non-interacting problem, three-quarters filling is a closed-shell case with double occupancy of all points designated by a solid marker. Half-filling is an open shell case with double occupancy of the solid circles and the remaining occupancy being some linear combination of half the solid diamonds. From Fig. 2, one sees that the Fermi energy of the  $\frac{3}{4}$  and completely full states are nearly equal.

When the lower band is  $\frac{1}{4}$ -filled, the number of electronic quasi-particles is much less than the number of lattice sites, making it unlikely that the Coulomb interaction  $U$  will induce an instability, because of the unlikely double occupancy of the f-levels. Also the density of states will most likely remain free-electron-like and small. We did not investigate

this filling. At  $\frac{1}{2}$ -filling, the number of quasi-particles equals the number of lattice sites and perfect nesting,<sup>11</sup> reminiscent of the Hubbard model, occurs and a similar anti-ferromagnetic insulating state is expected. We also did not investigate this filling at this time. We focused on fillings of  $\frac{3}{4}$  and higher.

At  $\frac{3}{4}$ -filling new possibilities exist. The likelihood of double occupancy is large because the number of quasi-particles is much larger than the number of lattice sites, and the density of states at  $E_F$  is large because of the dispersionless character of the band. If the interaction is strong, each f-state on the average will be occupied by a single electron with a nearly fully developed magnetic moment, and these moments will interact anti-ferromagnetically. The questions are, “Does a magnetic instability characterized by  $\mathbf{Q} = (\pi, 0)$  develop?” and “What is the nature of this state?”

When the lower band is full, a band gap exists. For a sufficiently large value of  $U$ , each f-orbital on the average will be singly occupied, the spins of these electrons will be arranged anti-ferromagnetically, and the gap will be enlarged. In this paper we will study the evolution of this state as we hole dope it towards the  $\frac{3}{4}$ -filled case where a magnetic state of a different character develops.

### III. CONSTRAINED-PATH MONTE CARLO METHOD

Our numerical method is extensively described and benchmarked elsewhere.<sup>6</sup> Here we only discuss its basic approximation. In the CPMC method, the ground-state wave function  $|\Psi_0\rangle$  is projected from a known initial wave function  $|\Psi_T\rangle$  by a branching random walk in an over-complete space of Slater determinants  $|\phi\rangle$ . In such a space, we can write  $|\Psi_0\rangle = \sum_{\phi} \chi(\phi)|\phi\rangle$ . The random walk produces an ensemble of  $|\phi\rangle$ , called random walkers, which represent  $|\Psi_0\rangle$  in the sense that their distribution is a Monte Carlo sampling of  $\chi(\phi)$ , that is, a sampling of the ground-state wave function.

To completely specify the ground-state wave function, only determinants satisfying  $\langle\Psi_0|\phi\rangle > 0$  are needed because  $|\Psi_0\rangle$  resides in either of two degenerate halves of the Slater

determinant space, separated by a nodal plane  $\mathcal{N}$  that is defined by  $\langle \Psi_0 | \phi \rangle = 0$ . The sign problem occurs because walkers can cross  $\mathcal{N}$  as their orbitals evolve continuously in the random walk. Asymptotically they populate the two halves equally. If  $\mathcal{N}$  were known, we would simply constrain the random walk to one half of the space and obtain an exact solution of Schrödinger’s equation. In the constrained-path QMC method, without *a priori* knowledge of  $\mathcal{N}$ , we use a trial wave function  $|\Psi_T\rangle$  and require  $\langle \Psi_T | \phi \rangle > 0$ . The random walk again solves Schrödinger’s equation in determinant space, but under an approximate boundary-condition. This is what is called the constrained-path approximation.

The quality of the calculation clearly depends on the quality of the trial wave function  $|\Psi_T\rangle$ . Since the constraint only involves the overall sign of its overlap with any determinant  $|\phi\rangle$ , it seems reasonable to expect the results to show some insensitivity to  $|\Psi_T\rangle$ . Through extensive benchmarking on the Hubbard model, it has been found that simple choices of this function can give very good results.<sup>6–9</sup>

Besides as starting point and as a condition constraining a random walker, we also use  $|\Psi_T\rangle$  as an importance function. Specifically we use  $\langle \Psi_T | \phi \rangle$  to bias the random walk into those parts of Slater determinant space that have a large overlap with the trial state. For all three uses of  $|\Psi_T\rangle$ , it clearly is advantageous to have  $|\Psi_T\rangle$  approximate  $|\Psi_0\rangle$  as closely as possible. Only in the constraining of the path does  $|\Psi_T\rangle \neq |\Psi_0\rangle$  in general generate an approximation.

All the calculations reported here are done with periodic boundary conditions. Mostly, we study closed shell cases, for which the corresponding free-electron wave function is non-degenerate and translationally invariant. In these cases, the free-electron wave function, represented by a single Slater determinant, is used as the trial wave function  $|\psi_T\rangle$ . (The use of an unrestricted Hartree-Fock wave function as  $|\psi_T\rangle$  produced no significant improvement in the results).

In particular, we represented the trial wavefunction as a single Slater determinant whose columns are the  $N_\sigma$  single-particle orbitals obtained from the exact solution of  $H_0$ . We chose the orbitals with lowest energies given by  $E_-^\sigma(\mathbf{k})$  and filled them up to a desired number of

electrons  $N_e$ .

$$|\psi_T\rangle = \prod_{\mathbf{k},\sigma} \alpha_{\mathbf{k},\sigma}^\dagger |0\rangle, \quad (7)$$

where  $|0\rangle$  represents a vacuum for electrons. Since our calculations were performed at or below a full lower band, only states from the lower band were used to construct the trial wavefunction.

In a typical run we set the average number of random walkers to 400. We performed 2000 Monte Carlo sweeps before we taking measurements, and we made the measurements in 40 blocks of 400 steps. By choosing  $\Delta\tau = 0.05$ , we reduced the systematic error associated with the Trotter approximation to be smaller than the statistical error. In measuring correlation functions, we performed between 20 to 40 back-propagation steps. The number of up and down electrons was always chosen equal  $N_\uparrow = N_\downarrow = N_e/2$ .

## IV. RESULTS

Our simulations were done for a  $6 \times 6$  lattice and lower-band fillings of 1,  $\frac{3}{4}$  and several values in between. At these fillings, we varied the repulsive on-site Coulomb interaction  $U$  to witness how the properties of a narrow band of non-interacting quasi-particles change when the interaction becomes large and how doping affects these properties. In particular we examined the effects of the interaction and doping on the electron and spin densities and the correlations between these densities.

### A. Filled Lower Band

We describe the electronic distribution in several ways. One is by its local (site) values  $\langle n_i^f \rangle$  and  $\langle n_i^d \rangle$ . Another is by its momentum distribution

$$\langle n(\mathbf{k}) \rangle = \langle n^\alpha(\mathbf{k}) \rangle + \langle n^\beta(\mathbf{k}) \rangle = \sum_{\sigma} \left[ \langle n_{\mathbf{k},\sigma}^\alpha \rangle + \langle n_{\mathbf{k},\sigma}^\beta \rangle \right] \quad (8)$$

An still another is by its total occupancies of the lower and upper bands

$$\begin{aligned}
\langle n^\alpha \rangle &= \frac{1}{N} \sum_{\mathbf{k}} \langle n^\alpha(\mathbf{k}) \rangle \\
\langle n^\beta \rangle &= \frac{1}{N} \sum_{\mathbf{k}} \langle n^\beta(\mathbf{k}) \rangle
\end{aligned} \tag{9}$$

Comparing and contrasting these different quantities as a function of the interaction strength is often very informative.

When  $U = 0$  and the lower band is completely full,  $\langle n^\alpha(\mathbf{k}) \rangle = 2$  and  $\langle n^\beta(\mathbf{k}) \rangle = 0$ . When  $U > 0$ , this uniformity changes, but we find only small changes. Near the  $\Gamma$  point in the Brillouin zone,  $\langle n(\mathbf{k}) \rangle$  becomes greater than 2. When this occurs,  $n^\beta(\mathbf{k})$  has become greater than zero at values of  $\mathbf{k}$  where  $\langle n^\alpha(\mathbf{k}) \rangle$  is nearly 2. In Fig. 4, we plot  $\langle n^\alpha(\mathbf{k}) \rangle$  and  $\langle n^\beta(\mathbf{k}) \rangle$  along the lines connecting the high symmetry points in the irreducible part of the Brillouin zone. By plotting the pieces of  $\langle n(\mathbf{k}) \rangle$  separately, we get an enhanced picture of how the quasi-particle picture changes. What Fig. 4 suggests, for example, is turning on the repulsive interaction moves some of the short wavelength electron momentum to longer wavelengths in presumably higher energy states. In other words, as  $U$  is increased, some of the itinerant character of the non-interacting quasi-particles is changed to a more localized one and examining the site-dependent expectation values of the electron occupancy becomes informative.

This transition is more explicitly seen in Fig. 5 which shows a nearly saturated moment

$$\langle S_f^z(i)^2 \rangle = \langle (n_{i,\uparrow}^f - n_{i,\downarrow}^f)^2 \rangle \approx 1 \tag{10}$$

developing on each f-orbital as  $U$  is increased. This observation with the additional observation of  $\langle n_i^f \rangle \approx 1$  and the use of the algebraic identity

$$\langle S_f^z(i)^2 \rangle = \langle n_i^f \rangle - 2\langle n_{i,\uparrow}^f n_{i,\downarrow}^f \rangle \tag{11}$$

implies that  $\langle n_{i,\uparrow}^f n_{i,\downarrow}^f \rangle = 0$  and thus demonstrates that a large  $U$  localizes a single electron on each f-orbital. The picture for the d-electrons differs. Here, when  $\langle n_i^d \rangle \approx 1$ ,  $\langle S_d^z(i)^2 \rangle \approx 0.5$ , and the identity

$$\langle S_d^z(i)^2 \rangle = \langle n_i^d \rangle - 2\langle n_{i,\uparrow}^d n_{i,\downarrow}^d \rangle \tag{12}$$

implies that  $\langle n_{i,\uparrow}^d n_{i,\downarrow}^d \rangle \approx \frac{1}{4}$ . Thus, the d-electrons do not sit one per site but instead show some itinerant character.

The spin-spin correlation function

$$S_{ff}(\mathbf{k}) = \frac{1}{N} \sum_{i,j} e^{i\mathbf{k}\cdot(\mathbf{R}_i - \mathbf{R}_j)} \langle (n_{i,\uparrow}^f - n_{i,\downarrow}^f)(n_{j,\uparrow}^f - n_{j,\downarrow}^f) \rangle = \frac{1}{N} \sum_{i,j} e^{i\mathbf{k}\cdot(\mathbf{R}_i - \mathbf{R}_j)} \langle S_f^z(i) S_f^z(j) \rangle \quad (13)$$

plotted in Fig. 6a, shows a strong enhancement of  $S_{ff}(\pi, \pi)$  occurring as  $U$  is increased. In contrast, the enhancement to  $S_{dd}(\pi, \pi)$ , shown in Fig. 6b, is much smaller. Additional insight follows from the spatial correlation functions. The function  $\langle S_f^z(i) S_f^z(j) \rangle$  for  $i \neq j$  shows long-range anti-ferromagnetic correlations. The magnitude of these correlations are a factor of 20 to 30 larger than those shown by  $\langle S_d^z(i) S_d^z(j) \rangle$  (for  $i \neq j$ ). The d-electrons are behaving as a collection of weakly anti-ferromagnet, rather itinerant electrons.

A large  $U$  separates the f and d-electrons into two coupled anti-ferromagnetic layers. To study the correlations between these layers, we calculated  $\langle S_f^z(i) S_d^z(j) \rangle$ . Figure 7 shows this function for a small and a large value of  $U$ . For the small value of  $U$ , when  $i = j$ , the correlation between the hybridized sites is negative; otherwise, it decays rapidly with the distance away from the orbital site in a manner reminiscent of the decaying correlations found in the single impurity Anderson model.<sup>12</sup> For a large value of  $U$ , when  $i = j$ , the correlation between hybridized sites is again negative; otherwise, it shows long-range anti-ferromagnetic oscillations. In general, the magnitude of spatial spin correlations between the d and f-electrons is about an order of magnitude larger than those between the d-electrons.

For all values of  $U$  studied, the expectation value of the net total magnetization was zero:

$$\langle S^z \rangle = \sum_i \langle S_d^z(i) + S_f^z(i) \rangle = 0 \quad (14)$$

From this and the fact that the ground state is an eigenstate of the total magnetization, the following constraints on the spatial spin correlations functions hold and were observed in the results of the simulations

$$\sum_i \langle S_f^z(i) S_f^z(j) \rangle = \sum_i \langle S_d^z(i) S_d^z(j) \rangle = - \sum_i \langle S_f^z(i) S_d^z(j) \rangle \quad (15)$$

Rewriting these equations

$$\begin{aligned}\langle S_f^z(j)^2 \rangle &= -\sum_i \langle S_f^z(i) S_d^z(j) \rangle - \sum_{i \neq j} \langle S_f^z(i) S_f^z(j) \rangle \\ \langle S_d^z(j)^2 \rangle &= -\sum_i \langle S_f^z(i) S_d^z(j) \rangle - \sum_{i \neq j} \langle S_d^z(i) S_d^z(j) \rangle\end{aligned}\quad (16)$$

shows that both the d and f-electrons participate in the spin compensation of the local d and f-moments and that this compensation is qualitatively different in the PAM from the spin compensation in the single-impurity model.<sup>12,13</sup> In the single-impurity model, the impurity spin compensation formula is<sup>12</sup>

$$\langle S_f^z(j)^2 \rangle = -\sum_i \langle S_d^z(i) S_f^z(j) \rangle \quad (17)$$

This equation is not even approximately obeyed for the PAM. In the PAM compensation of the local moment definitely involves the moments on the other orbitals, not just the d electrons. This possibility was suggested by Nozières<sup>14</sup> for non-dilute Kondo alloys and noted by several authors<sup>15,16</sup> in the context of dynamical mean-field calculations for the PAM. We remark that spin compensation holds for all dopings and values of  $U$  as long as  $\langle S^z \rangle = 0$ , and while it is consistent with a singlet ground state, it is not proof of a singlet ground state.<sup>13</sup> In the Kondo regime, as in the single-impurity model, short-range spin correlations act to compensate the f-moments; in the anti-ferromagnetic regime, long-range correlations act.

Similar correlations functions can be computed for the charge. For example,

$$C_{ff}(\mathbf{k}) = \frac{1}{N} \sum_{i,j} e^{i\mathbf{k} \cdot (\mathbf{R}_i - \mathbf{R}_j)} \left[ \langle (n_{i,\uparrow}^f + n_{i,\downarrow}^f)(n_{j,\uparrow}^f + n_{j,\downarrow}^f) \rangle - \langle n_{i,\uparrow}^f + n_{i,\downarrow}^f \rangle \langle n_{j,\uparrow}^f + n_{j,\downarrow}^f \rangle \right] \quad (18)$$

The magnitude of these correlation functions is 2 to 3 orders smaller than the magnitude of  $S_{ff}(\pi, \pi)$ . Shown in Figs. 8a and 8b are the charge-charge correlation functions for the filled lower band case. For the d-electrons, increasing  $U$  increases the magnitude of the charge correlations slightly, and these correlations are the strongest near  $(\pi, \pi)$ . Increasing  $U$  suppresses the f-electron charge correlations. In general, the changes in these correlations are small relative to the  $U = 0$  values. The behavior of the charge-charge correlation

functions as a function of  $U$  is qualitatively and quantitatively the same at other fillings and so these functions will not be discussed further.

### B. Incommensurate Fillings

When we start hole doping away from the filled lower band, the principal effect is the eventual destruction of the anti-ferromagnetic correlations. For small  $U$ , where these correlations do not exist, doping does not qualitatively change the behavior of the physical quantities we computed. The principal change is a reduction in the value of  $\langle n^\beta(\mathbf{k}) \rangle$ , that is, the removal of charge from the upper band. The lattice is a “charge reservoir” for the orbitals. When  $U$  is large, doping reduces the value of  $\langle n_i^d \rangle$ , that is, removes electrons from the lattice sites.

At large  $U$  the most significant change caused by the doping is the immediate and significant reduction of the magnitude of the long-range spatial correlations of the spins. To be more specific, fixing  $U$  at a value for which we found anti-ferromagnetism in the full lower band case, then to our statistical accuracy we found that this anti-ferromagnetism disappeared by a filling of 33 up and 33 down electrons. Strong local moments on the orbitals, however, remained as in general we find that for a fixed value of  $U$  the magnitude of the moment is only a weak function of the doping. Doping mainly affects the nature of the indirect exchange mechanism that induces the anti-ferromagnetism. In contrast to the two-dimensional Hubbard model, the doping did not shift the peak in the spin-spin correlation from the  $(\pi, \pi)$  point to the incommensurate points  $(\pi \pm q, 0)$  and  $(0, \pi \pm q)$ .<sup>17</sup>

After the anti-ferromagnetic correlations are destroyed, continued doping changes the qualitative features of the computed quantities change very little. At large  $U$ , local moments still exist, the orbitals are singly-occupied, and the remaining electrons show free-electron-like spin-spin and charge-charge correlations. Short-range spin and charge correlations exist as evidenced by the respective correlation functions showing broad peaks at values of  $\mathbf{k}$  not equal to  $(0, 0)$  or  $(\pi, 0)$ . The height of these peaks are orders of magnitude smaller than the

height of the  $(\pi, \pi)$  peak that existed for the large values of  $U$  in the full lower band case. In Figs. 9 and 10 we present some of the properties of a system with 31 up and 31 down electrons.

### C. Three-quarters Filled

At large  $U$  and  $\frac{3}{4}$ -filling, a peak in the spin-spin correlation function dramatically appears at  $\mathbf{k} = (\pi, 0)$ . We will attribute this peak to the formation of a resonating pair of  $\mathbf{Q} = (\pi, 0)$  and  $\mathbf{Q}' = (0, \pi)$  spin-density waves. The behavior of the system exhibits several other characteristics different from those found at other fillings. At this filling, when  $U = 0$ ,  $\langle n_i^f \rangle \approx 1$  and  $\langle n_i^d \rangle \approx 0.5$ , and double occupancy of the f-orbitals and lattice sites is small. A large  $U$  is not needed to induce single occupancy of the f-orbitals. Increasing  $U$  actually slightly decreases the f occupancy and slightly increases the d occupancy.

In Fig. 11, we show the electron momentum distribution. As  $U$  is increased, two effects occur. The first effect is the expected development of a nearly saturated moment on each f-orbital (Fig. 12). The second effect is the apparent disappearance of the quasi-particle residue<sup>18</sup>

$$Z(\mathbf{k}_F) = n(\mathbf{k} \rightarrow \mathbf{k}_F^+) - n(\mathbf{k} \rightarrow \mathbf{k}_F^-) \quad (19)$$

The Fermi surface is becoming less apparent, if it still exists.

The  $\mathbf{Q} = (\pi, 0)$  peak in the spin-spin correlation is shown in Fig. 13. The remaining correlation functions are similar in magnitude and features as for the other dopings. However, when  $S_{ff}(\mathbf{k})$  peaks, there was no peak in  $S_{dd}(\mathbf{k})$ . Although we will not explicitly demonstrate that the peak in  $S_{ff}(\mathbf{k})$  signifies a state of long-range order, its presence is consistent with an ordered state where the spins are aligned ferromagnetically in rows and anti-ferromagnetically in columns. There are two such alignments and they correspond to a commensurate spin-density wave characterized by  $\mathbf{Q} = (\pi, 0)$  and its symmetry equivalent  $(0, \pi)$ . We will now argue that the state we see is a linear combination of both spin-density wave states, a state which we call a resonating spin-density wave (RSDW) state.

If we look at the spatial spin-spin correlation function  $\langle S_f^z(i)S_f^z(j) \rangle$ , we find strong correlations existing between points on the same sub-lattice but very weak ones between points on the different sub-lattices of the bi-partite square lattice. We argue that the correlations between sub-lattices are in fact zero. We base the argument on the additional computation of the transverse spin-spin correlation function,  $\frac{1}{2}\langle S_f^+(i)S_f^-(j) + S_f^-(i)S_f^+(j) \rangle$ . As noted by Hirsch,<sup>19</sup> this correlation function can often be computed with smaller statistical error than the longitudinal function. We found this to be the case here. The predicted correlations (Table 1) between the sub-lattices were five times smaller than those found with the longitudinal correlation function and were the same size as the statistical error. Hence to the accuracy of our simulation they are zero.

The observed state is consistent with the ground-state resonating between two spin-density wave states, represented schematically for a  $3 \times 3$  lattice as

$$\begin{array}{rcc}
\uparrow \uparrow \uparrow & \uparrow \downarrow \uparrow & \uparrow 0 \uparrow \\
\downarrow \downarrow \downarrow + \uparrow \downarrow \uparrow & = & 0 \downarrow 0 \\
\uparrow \uparrow \uparrow & \uparrow \downarrow \uparrow & \uparrow 0 \uparrow
\end{array} \tag{20}$$

We could equally well depict the process as

$$\begin{array}{rcc}
\uparrow \uparrow \uparrow & \uparrow \downarrow \uparrow & 0 \uparrow 0 \\
\downarrow \downarrow \downarrow - \uparrow \downarrow \uparrow & = & \downarrow 0 \downarrow \\
\uparrow \uparrow \uparrow & \uparrow \downarrow \uparrow & 0 \uparrow 0
\end{array} \tag{21}$$

Either process produces diagonally-crossed anti-ferromagnetic chains separated by diagonally-crossed chains with no spins. We argue that  $\langle S_f^z(i) \rangle = 0$  is produced by linear combinations of the two SDW states and their translational symmetry equivalents. We also observe the equality of the longitudinal and transverse correlation functions on an element by element basis which suggests that the f-electrons are in a singlet state.

As we hole dope away from this unusual state, the peak height at  $(\pi, 0)$  decreases and the peak width broadens. We did not extensively investigate these fillings.

## V. CONCLUSIONS

We studied the effects of hole doping on spin correlations in the periodic Anderson model, mainly at the full and three-quarters-full lower bands cases. In the full lower band case, strong anti-ferromagnetism develops when the  $U$  becomes comparable to the quasi-particle band width. In the three-quarters filled case, a novel kind of spin correlation develops between the moments of the f-orbitals that is consistent with the resonance between a  $(\pi, 0)$  and a  $(0, \pi)$  spin-density wave. In this state, which we call a resonant spin-density wave (RSDW) state, we also find that the spins on the different sublattices of the bipartite square lattice appear uncorrelated. Hole doping away from the completely full case rapidly destroys the long-range anti-ferromagnetic correlations, in a manner reminiscent of the destruction of anti-ferromagnetism in the Hubbard model. In contrast to the Hubbard model, the doping does not shift the peak in the magnetic structure factor from the  $(\pi, \pi)$  position. Particle and hole doping away from the three-quarters full case was not extensively studied, but doping appears to destroy this state relatively rapidly. At dopings intermediate to the full and three-quarters full case, only weak spin correlations exist.

At a given doping, we found that increasing  $U$  develops a strong local magnetic moment on each f-orbital, mixes the upper and lower band quasi-particles, promotes the single occupancy of the f-orbitals, and pushes the remainder of the electrons onto the lattice sites. These lattice electrons appear free-electron-like. In the filled band case, they showed only minor correlations with the anti-ferromagnetic order that develops among the moments on the orbitals; at three-quarters filling, they show no correlation with the magnetic structure on the orbitals. When  $\langle S^z \rangle = 0$ , we noted that both the d and f-electrons participate in the screening of the d and f-moments.

We did not do the finite size scaling necessary to establish long-range order at the two central fillings we studied. For the full lower band case, Vekić et al.<sup>3</sup> did this study for the symmetric model and demonstrated long-range order. We see no reason why long-range order would be absent when we increased  $U$  and moved the model towards the symmetric

case. We are also leaving the finite-size scaling study of the state at three-quarters filling to future work, when we can study this state and the effects of doping on it in more detail. Whether the RSDW state is one of long-range order is an open question. We did do several short simulations for a  $8 \times 8$  lattice, which requires about an order of magnitude more computer time than for the  $6 \times 6$  case. The peak in  $S_{ff}(\mathbf{k})$  at  $(\pi, 0)$  persisted, but our statistical error increased more than its height. A Hartree-Fock calculation also exhibited the peak. We remark that for the  $8 \times 8$  lattice,  $\frac{3}{4}$ -filling is not a closed shell case, and for such cases our measured quantities in general have larger statistical errors than for closed shell cases. We also are leaving to a future study the presence of charge and spin gaps. Although delicate, the computation of these gaps is within the capability of our numerical method. In the future, it would also be interesting to explore the half-full lower band case. This filling corresponds to one electron per site and seems marginal for the development of strong electronic correlation phenomena. If  $U$  is large, some question to ask include, What is the nature of induced indirect exchange interaction? Do any anti-ferromagnetic correlations ever develop? and Does the PAM act like a half-filled Hubbard model?<sup>14,15</sup>

### ACKNOWLEDGMENTS

This work was supported by the Department of Energy. Very helpful conversations with B. Brandow, M. Guerrero, M. Jarrell, and G. Ortiz are gratefully acknowledged.

## REFERENCES

- <sup>1</sup> T. Saso and Y. Seino, J. Phys. Soc. Jpn. **55**, 3729 (1986); T. Saso, Physica B & C **148**, 95 (1987).
- <sup>2</sup> Y. Zhang and J. Callaway, Phys. Rev. B **38**, 641 (1988).
- <sup>3</sup> M. Vekić, J. W. Cannon, D. J. Scalapino, R. T. Scalettar, and R. L. Sugar, Phys. Rev. Lett. **74**, 2367 (1995).
- <sup>4</sup> P. A. Lee, T. M. Rice, J. W. Serene, L. J. Sham, and J. W. Wilkins, Comments Condens. Matter Phys. **12**, 99 (1986).
- <sup>5</sup> S. Doniach, Physica **91B**, 231 (1977).
- <sup>6</sup> Shiwei Zhang, J. Carlson and J. E. Gubernatis, Phys. Rev. Lett., **74**, 3652 (1995); Phys. Rev. B, **55**, 7464 (1997).
- <sup>7</sup> Shiwei Zhang, J. Carlson and J. E. Gubernatis, Phys. Rev. Lett. **78**, 4486 (1997).
- <sup>8</sup> M. Guerrero, J. E. Gubernatis, Shiwei Zhang, Phys. Rev. B, to appear (cond-mat/9711125).
- <sup>9</sup> J. Bonča, J. E. Gubernatis, M. Guerrero, E. Jeckelmann, S. R. White, Phys. Rev. B RC, submitted (cond-mat/9712018).
- <sup>10</sup> E. Y. Loh, Jr. and J. E. Gubernatis, in *Electronic Phase Transitions*, edited by W. Hanke and Yu. V. Kopayev (Elsevier-Science, Amsterdam, 1991).
- <sup>11</sup> C. P. Enz, *A Course on Many-Body Theory Applied to Solid-State Physics* (World Scientific, Singapore, 1992), p. 344.
- <sup>12</sup> J. E. Gubernatis, J. E. Hirsch, and D. J. Scalapino, Phys. Rev. B **35**, 8478 (1987).
- <sup>13</sup> R. Blankenbecler, J. R. Fulco, W. Gill, and D. J. Scalapino, Phys. Rev. Lett. **58**, 411 (1987).

- <sup>14</sup> P. Nozières, *Ann. Phys. (Paris)* **10**, 19 (1985).
- <sup>15</sup> M. Jarrell, *Phys. Rev. B* **51**, 7419 (1995); A. J. Arko, P. S. Riseborough, A. B. Andrews, J. J. Joyce, A. Tahvildar-Zadeh, and M. Jarrell, in *Handbook on the Physics and Chemistry of Rare Earths*, edited by K.A. Gschneidner, Jr. and LeRoy Eyring, (North-Holland, Amsterdam, 1999), vol. 26, to appear.
- <sup>16</sup> B. Kyung, cond-mat/9802142.
- <sup>17</sup> N. Fukuwara and M. Imada, *J. Phys. Soc. Jpn.* **61**, 3331 (1992).
- <sup>18</sup> D. Pines, *The Many-Body Problem* (Benjamin, New York, 1961), p. 34.
- <sup>19</sup> J. E. Hirsch, *Phys. Rev. B* **35**, 1851 (1987).

## FIGURES

FIG. 1. The Brillouin zone of a square lattice. The points  $\Gamma$ , X, and M are high symmetry points. The irreducible part of the zone is the triangular region they define.

FIG. 2. The solid lines are the band structure of the non-interacting model for  $\epsilon_f = -2$  and  $V = \frac{1}{2}$ . The dashed line is the tight-binding band shifted to match the value of the upper band at the point M.

FIG. 3. The points in the first Brillouin zone for a  $6 \times 6$  lattice. The dashed lines is the fully nested Fermi surface for the half-filled case. The thick solid lines represent lines of nesting for a  $\mathbf{Q} = (\pi, 0)$  spin-density wave. Three-quarters filling corresponds to double occupancy of the points denoted by filled markers.

FIG. 4. Electron momentum density as a function of  $\mathbf{k}$  for the filled lower band as a function of  $U$ . The solid lines are for  $n_\alpha(\mathbf{k})$  and the dashed lines for  $n_\beta(\mathbf{k})$ .

FIG. 5. For the filled lower band,  $\langle n_i^d \rangle$ ,  $\langle n_i^f \rangle$ ,  $\langle n^\alpha \rangle$ ,  $\langle n^\beta \rangle$ ,  $\langle S_f^z(i)^2 \rangle$ , and  $\langle S_d^z(i)^2 \rangle$  as a function of  $U$ .

FIG. 6. Spin-spin correlation functions as a function of wavenumber and  $U$  for the filled band case. (a)  $S_{ff}(\mathbf{k})$ ; (b)  $S_{dd}(\mathbf{k})$ .

FIG. 7. Spin-spin correlation function  $\langle S_d^z(i)S_f^z(j) \rangle$  for the filled band case as a function of distance between high symmetry points in the unit cell. (a)  $U = 1$ ; (b)  $U = 2.5$ .

FIG. 8. Charge-charge correlation functions as a function of wavenumber and  $U$  for the filled band case. (a)  $C_{ff}(\mathbf{k})$ ; (b)  $C_{dd}(\mathbf{k})$ .

FIG. 9. Electron momentum density as a function of  $\mathbf{k}$  for a filling of 31 up and 31 down electrons as a function of  $U$ . The solid lines are for  $n_\alpha(\mathbf{k})$  and the dashed lines for  $n_\beta(\mathbf{k})$ .

FIG. 10. For 31 up and 31 down electrons,  $\langle n_i^d \rangle$ ,  $\langle n_i^f \rangle$ ,  $\langle n^\alpha \rangle$ ,  $\langle n^\beta \rangle$ ,  $\langle S_f^z(i)^2 \rangle$ , and  $\langle S_d^z(i)^2 \rangle$  as a function of  $U$ .

FIG. 11. Electron momentum density as a function of  $\mathbf{k}$  for a  $\frac{3}{4}$  filling as a function of  $U$ . The solid lines are for  $n_\alpha(\mathbf{k})$  and the dashed lines for  $n_\beta(\mathbf{k})$ .

FIG. 12. For the  $\frac{3}{4}$ -filled lower band,  $\langle n_i^d \rangle$ ,  $\langle n_i^f \rangle$ ,  $\langle n^\alpha \rangle$ ,  $\langle n^\beta \rangle$ ,  $\langle S_f^z(i)^2 \rangle$ , and  $\langle S_d^z(i)^2 \rangle$  as a function of  $U$ .

FIG. 13. Spin-spin correlation functions as a function of wavenumber and  $U$  for the  $\frac{3}{4}$ -filled band case. (a)  $S_{ff}(\mathbf{k})$ ; (b)  $S_{dd}(\mathbf{k})$ .

## TABLES

TABLE I. The spatial spin-spin correlation function  $\langle S_f^z(i)S_f^z(j) \rangle$  for a  $6 \times 6$  lattice. Given are only the lattices sites in one quadrant of the super cell and these sites labeled by the point  $(i, j)$  starting from the cell center  $(0, 0)$ . The numbers in parenthesis are the estimated statistical errors of the last digits.

$(i, j)$	0	1	2	3
0	0.893(0)	0.000(6)	0.152(38)	-0.006(4)
1	0.002(7)	-0.284(45)	0.000(17)	-0.151(50)
2	0.157(78)	0.003(11)	0.109(30)	-0.001(6)
3	-0.010(7)	-0.131(26)	-0.003(7)	-0.087(35)

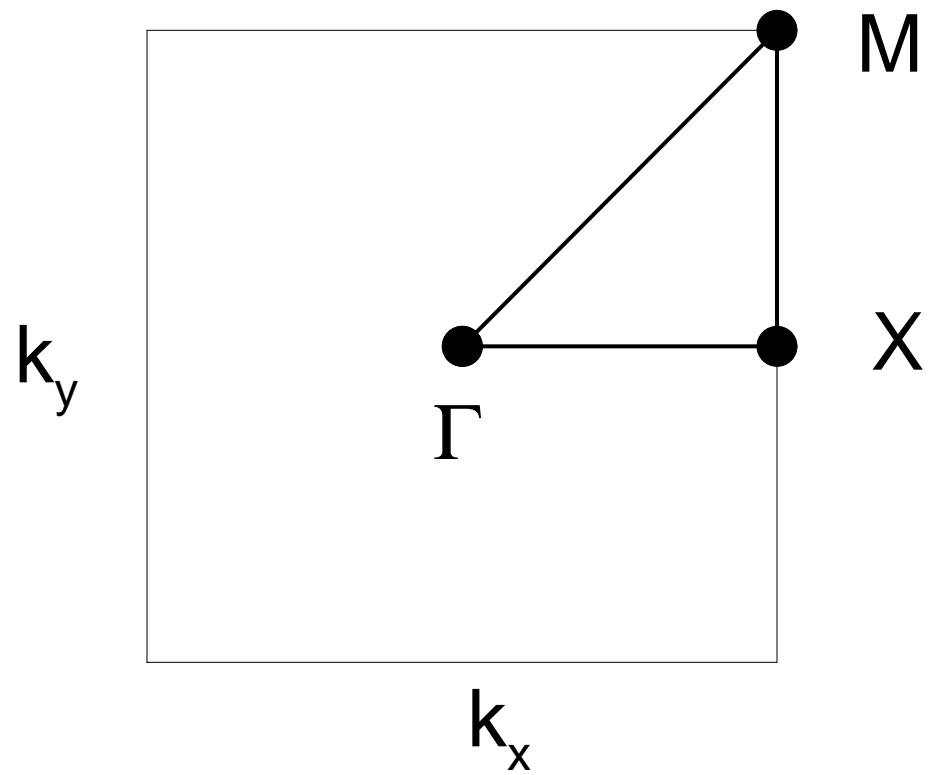


fig 1

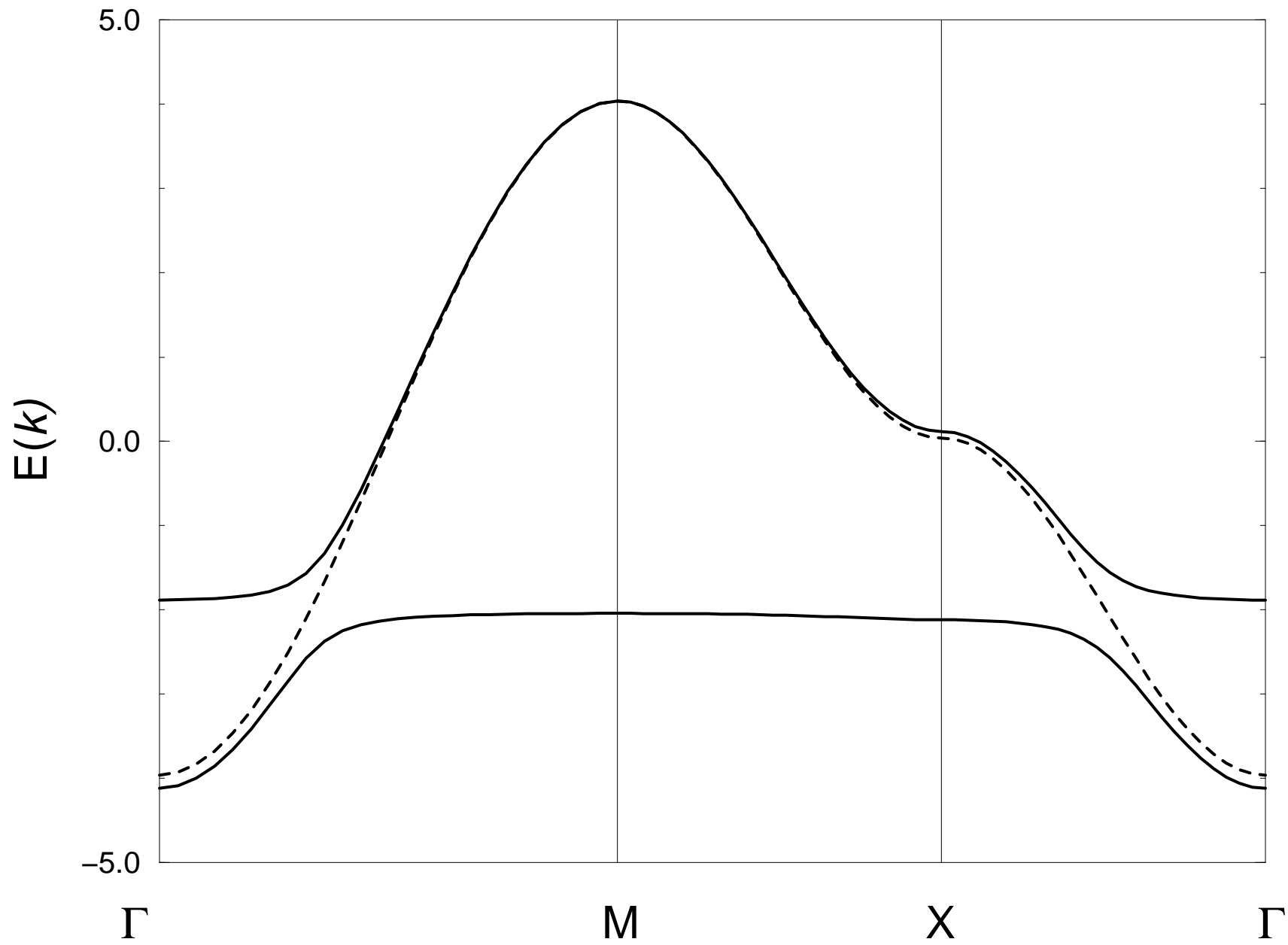


fig 2

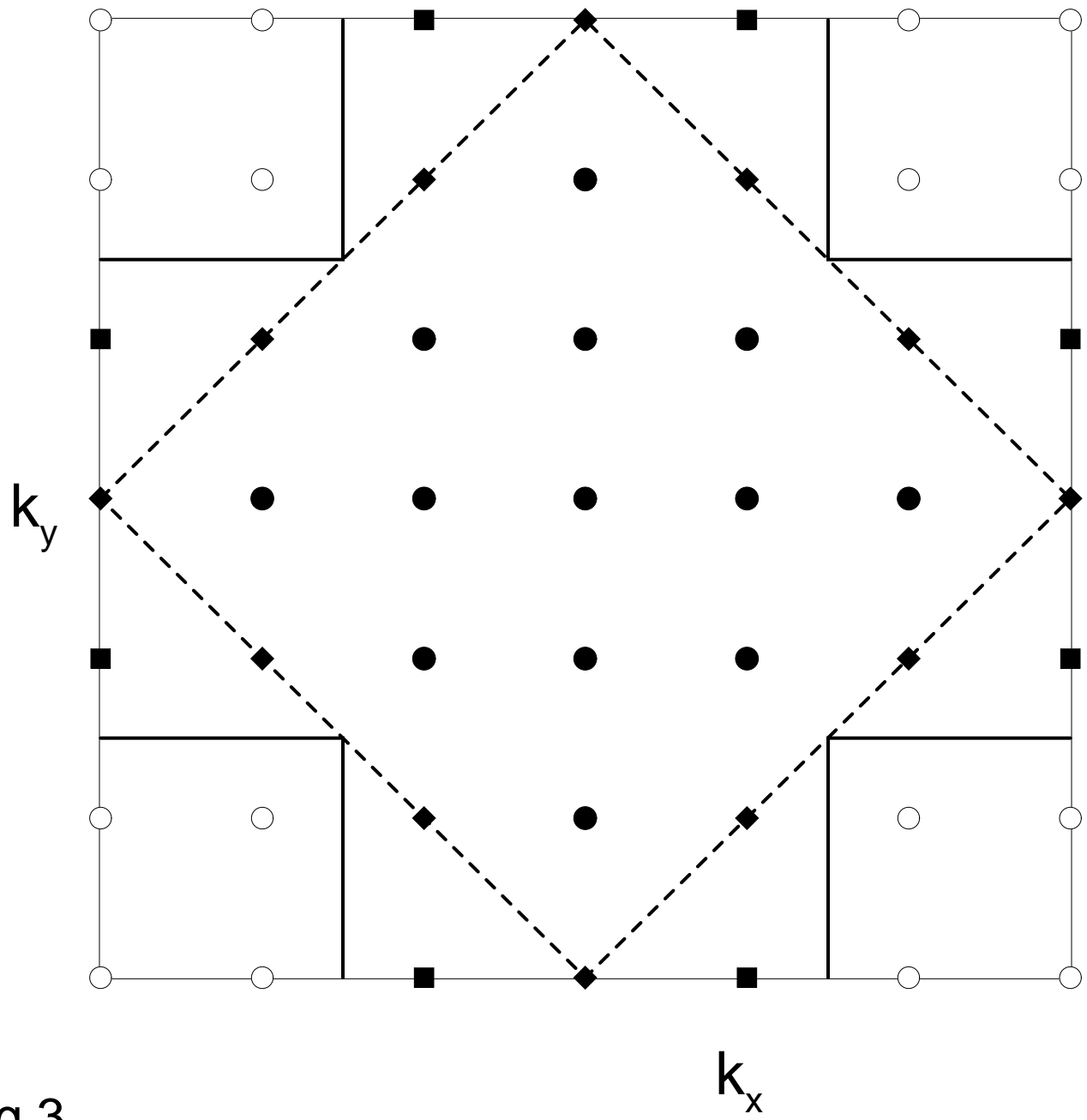


fig 3

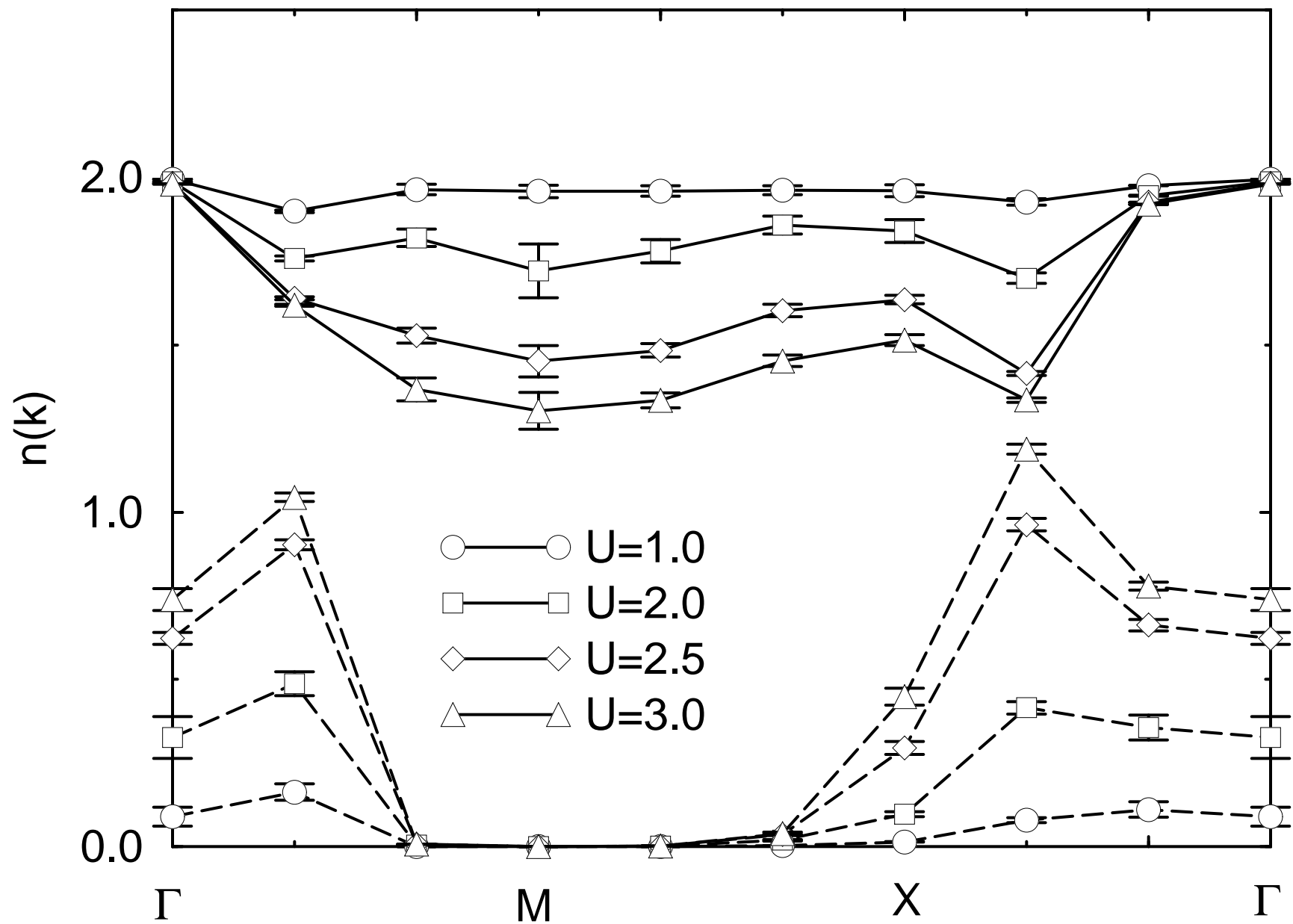


fig 4

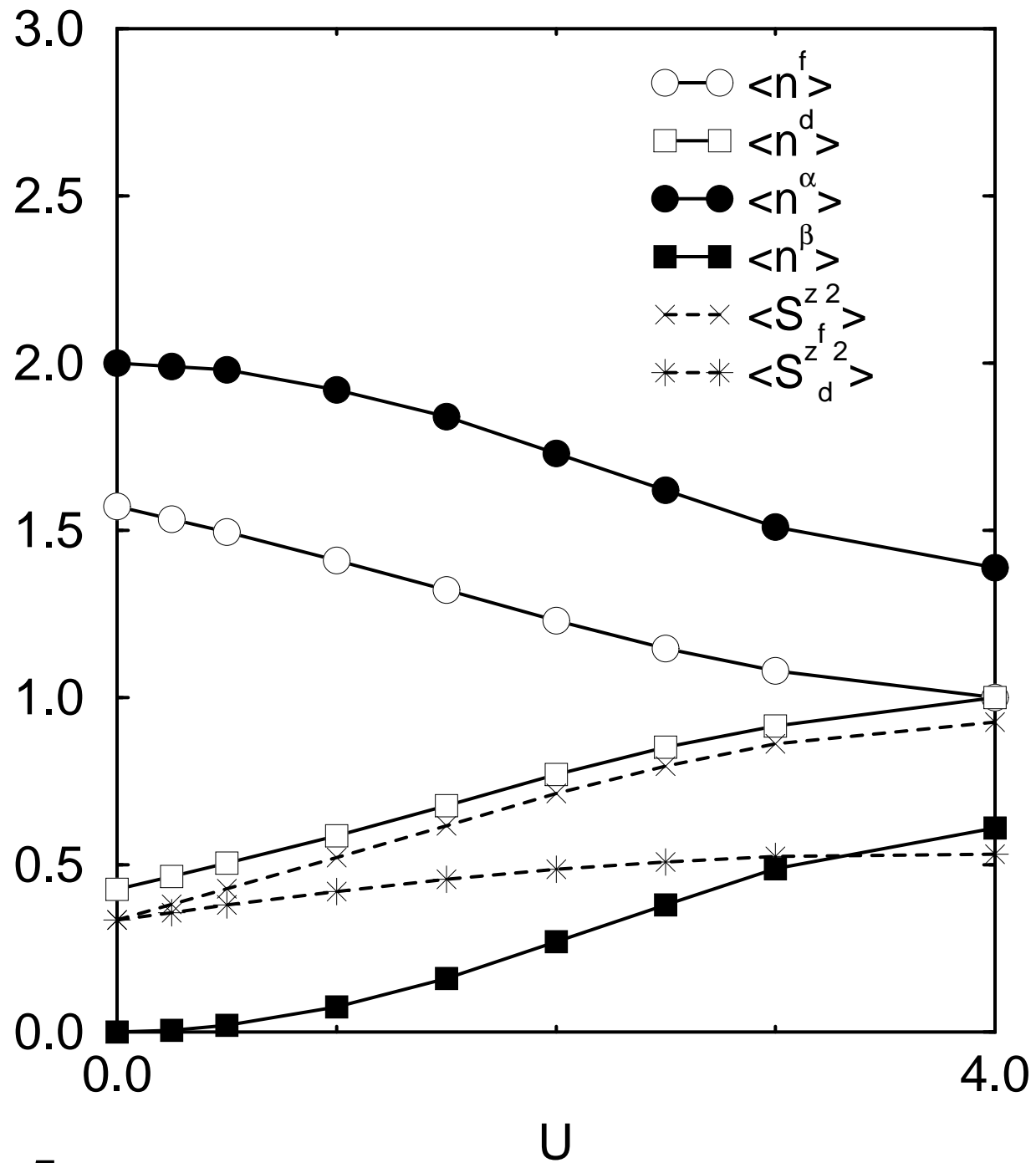


fig 5

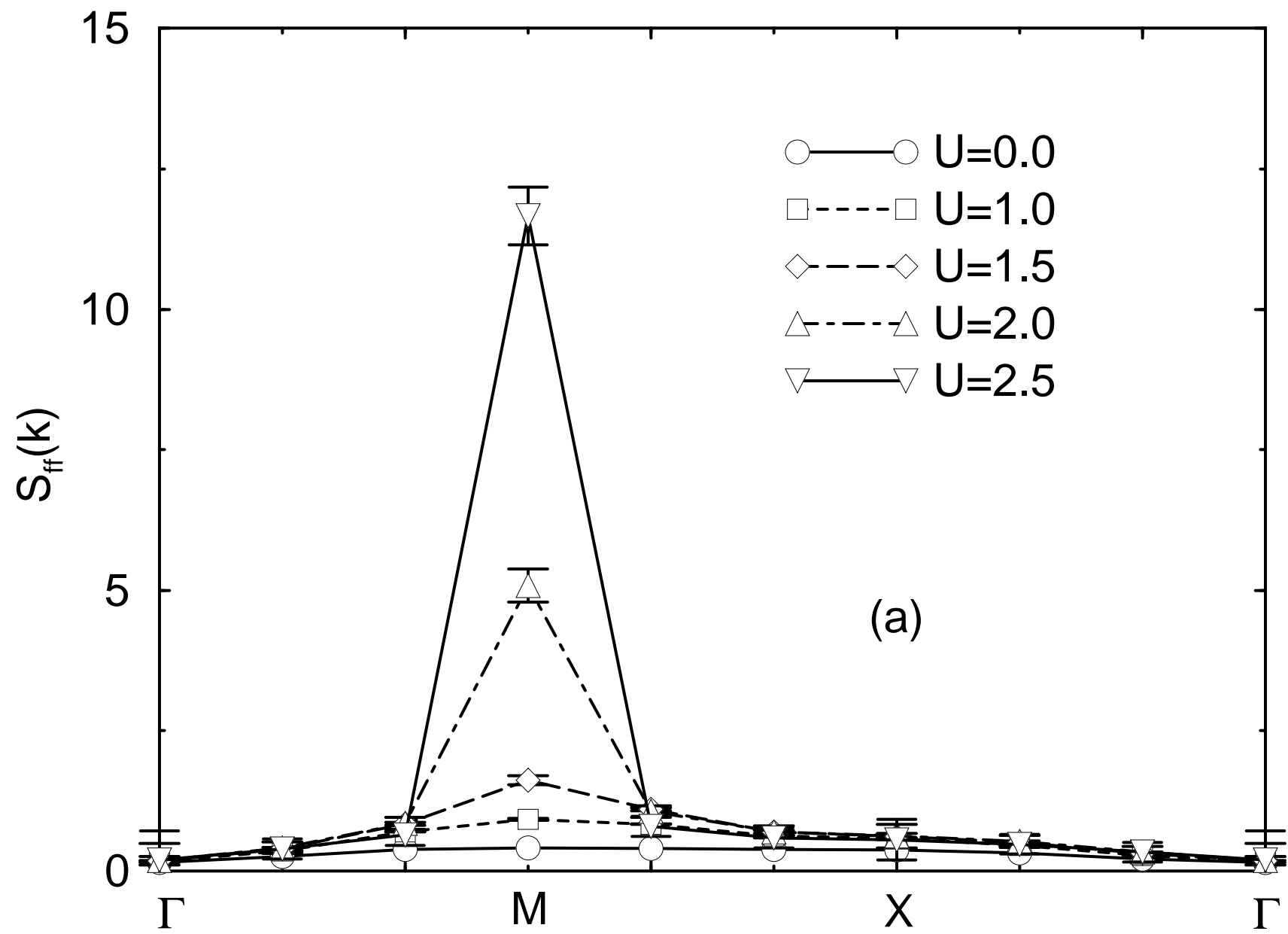


fig 6a

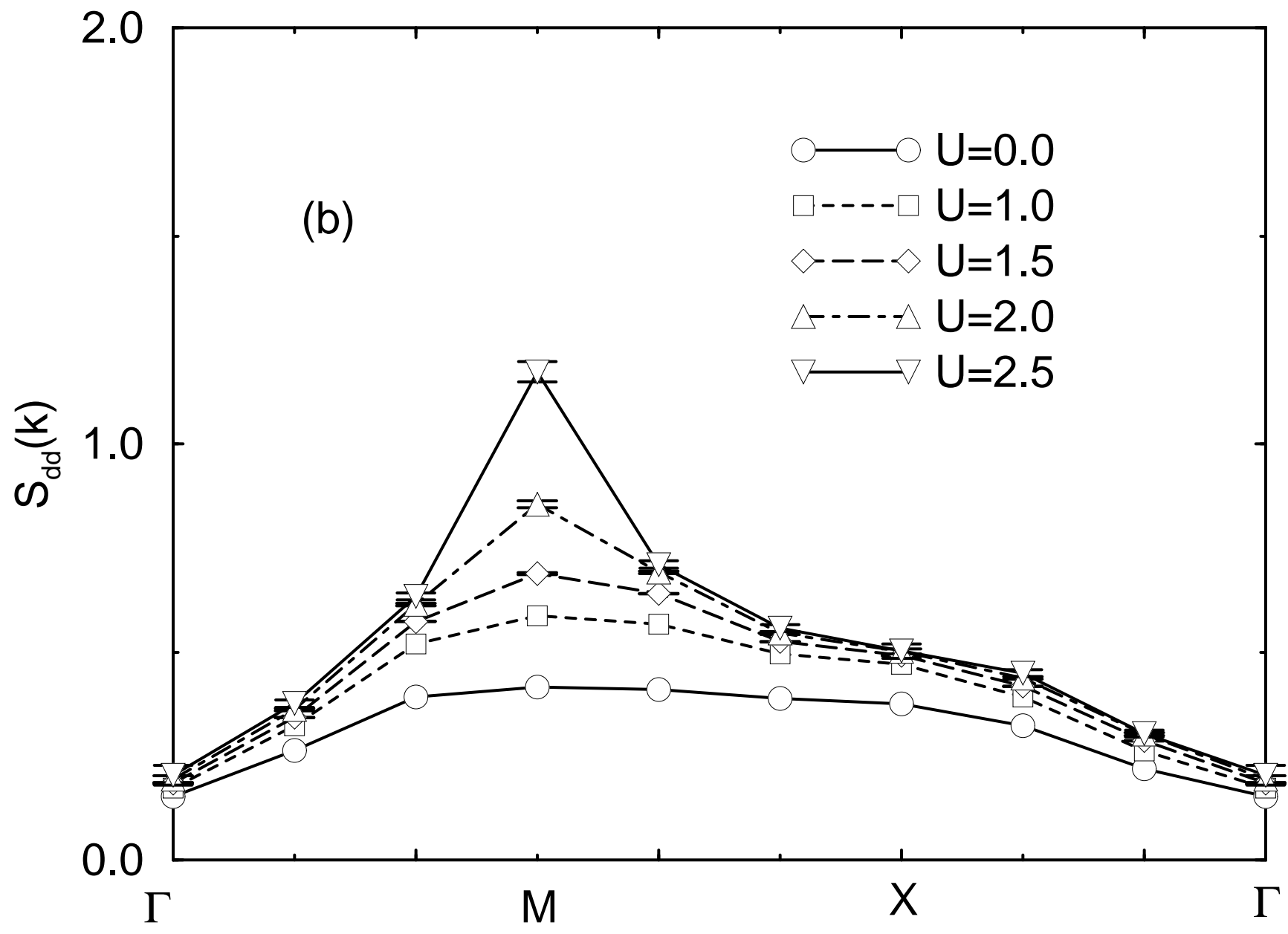


fig 6b

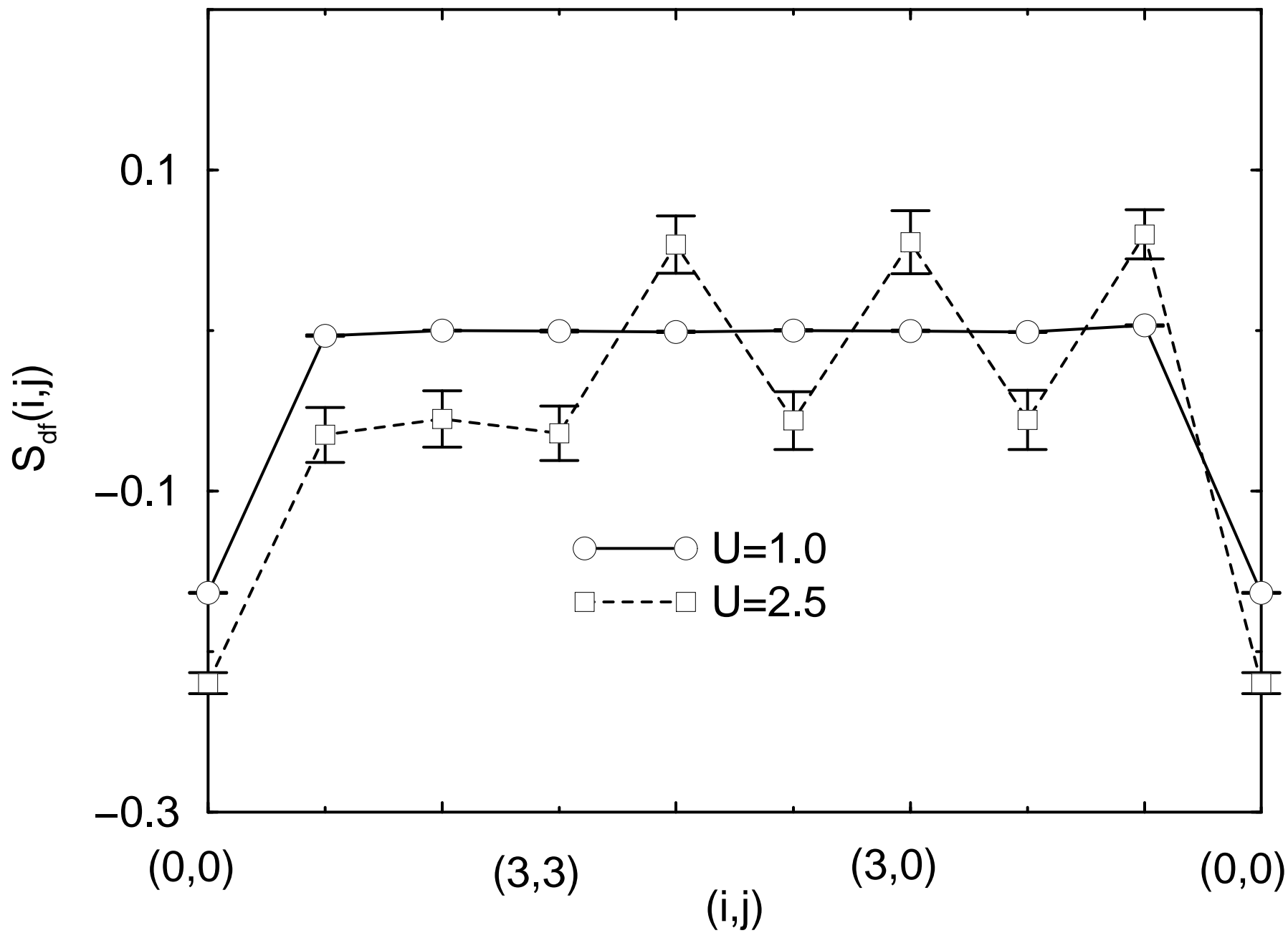


fig 7

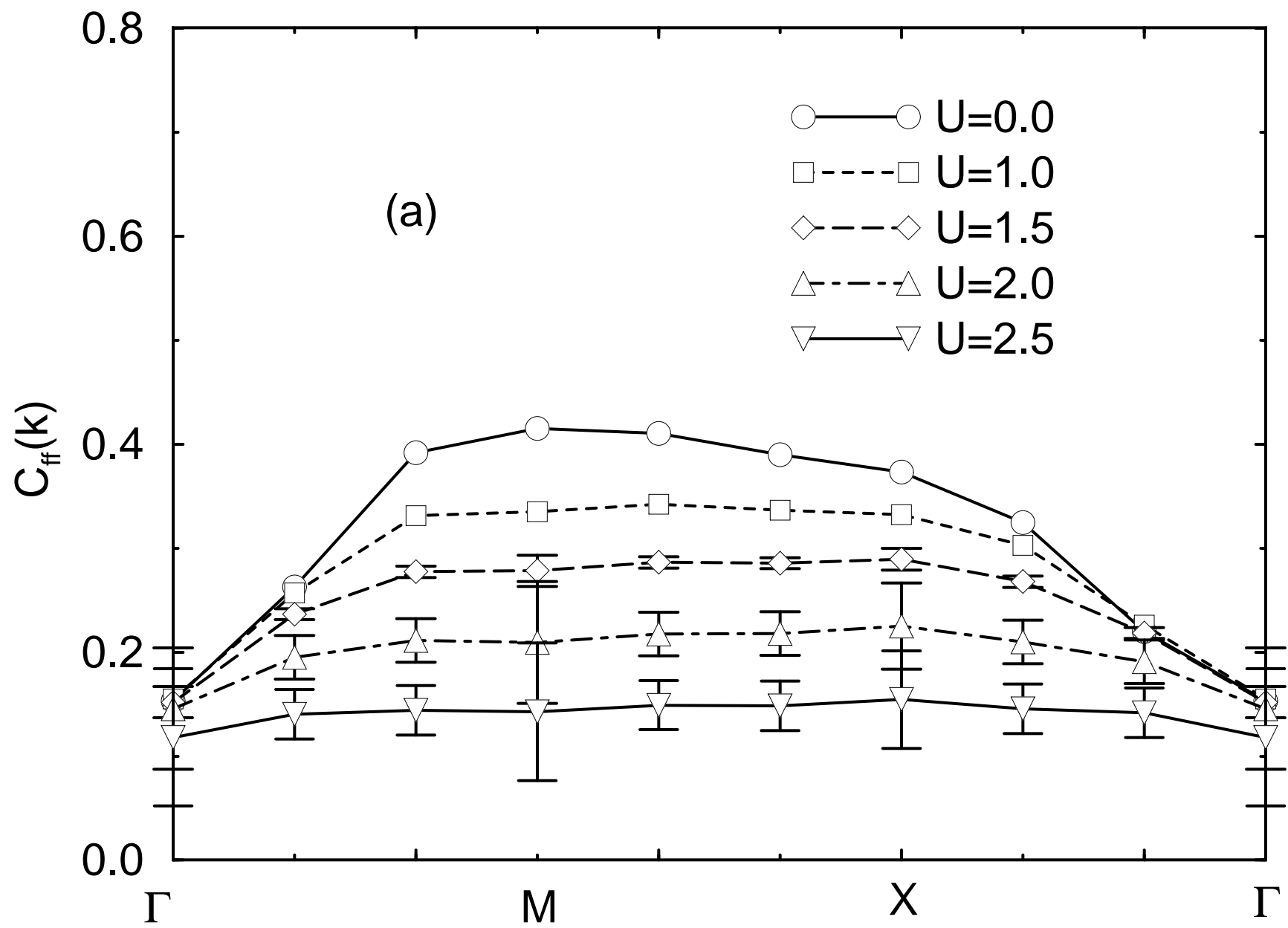


fig 8a

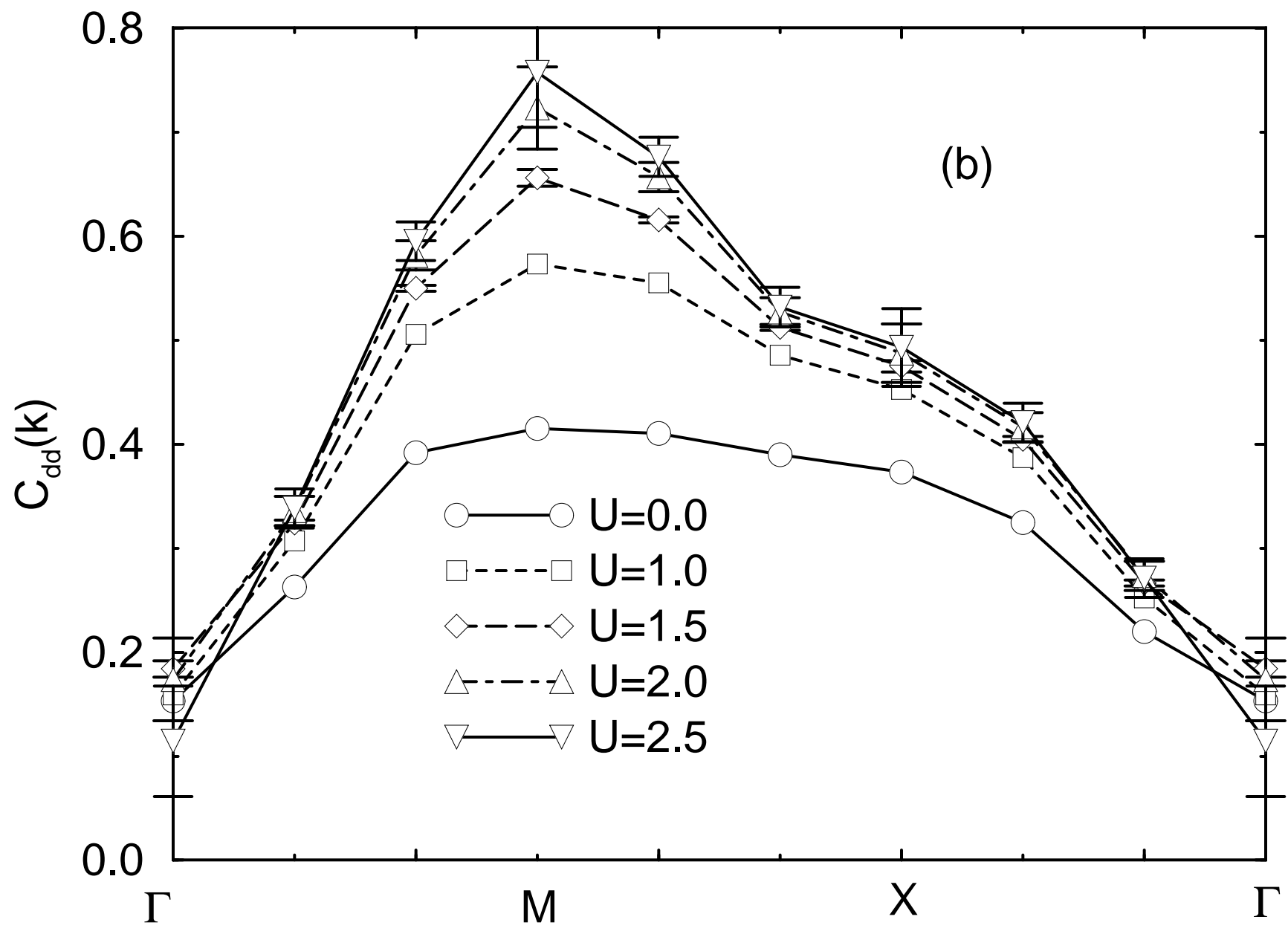


fig 8b

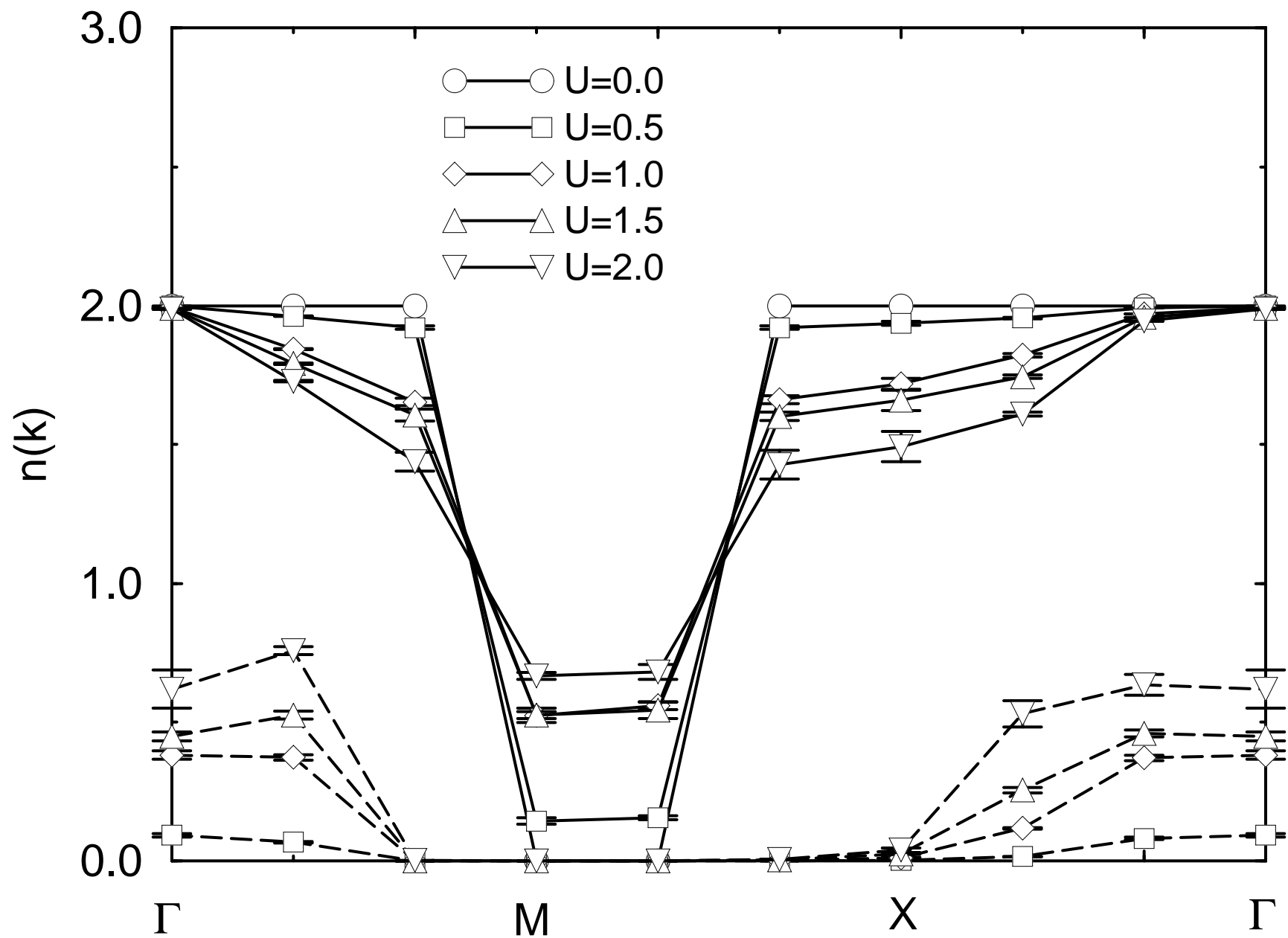


fig 9

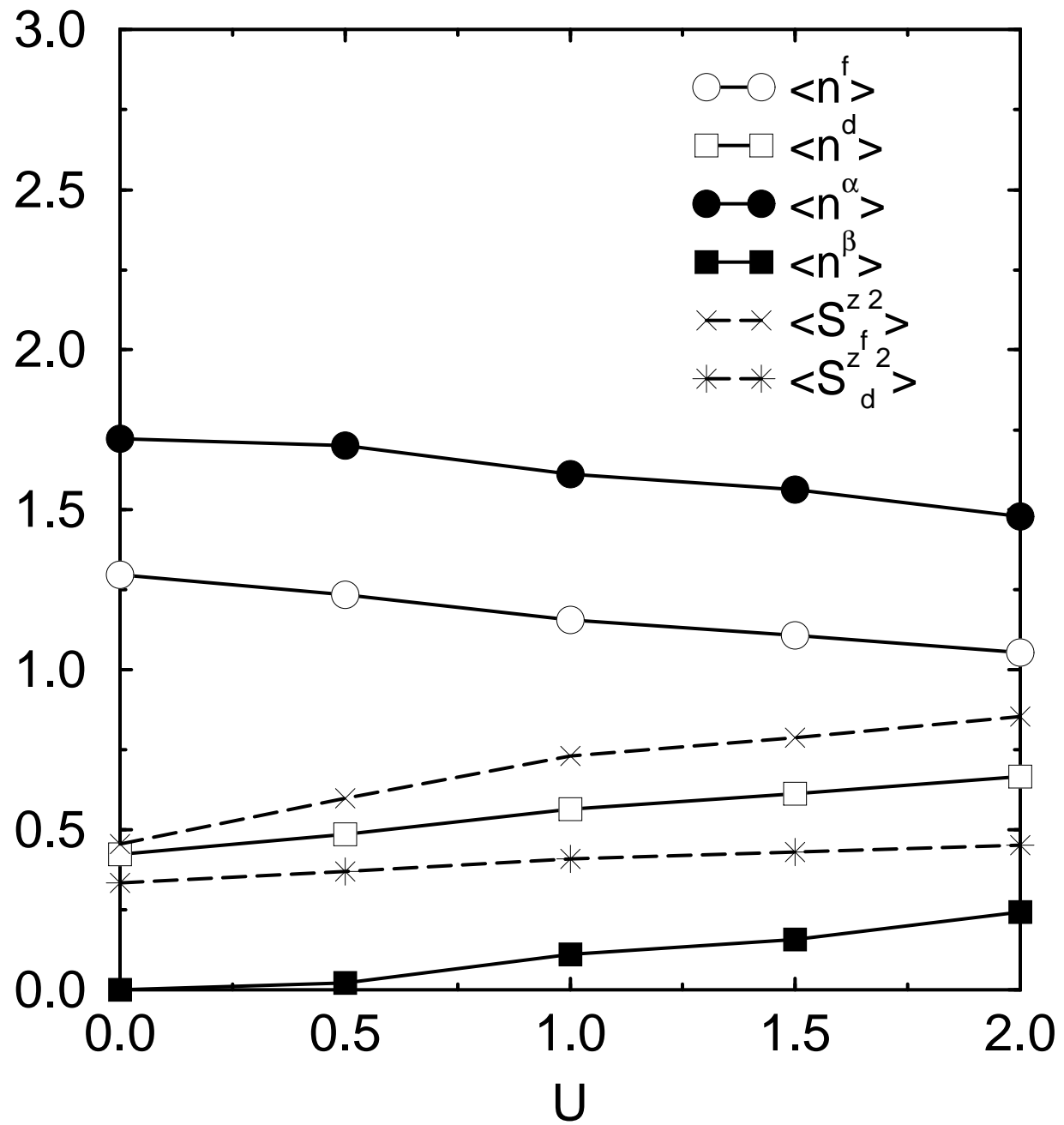


fig 10

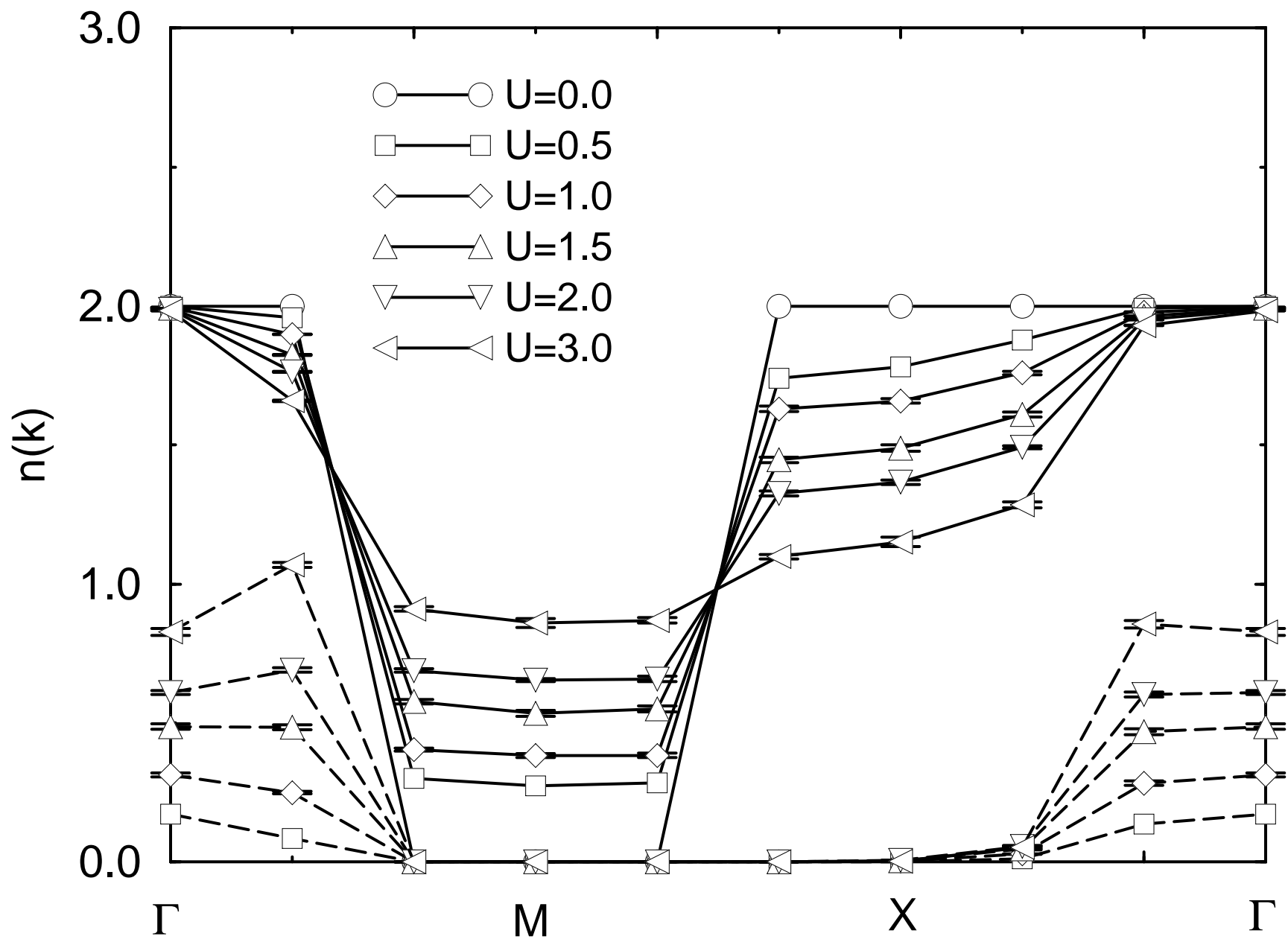


fig 11

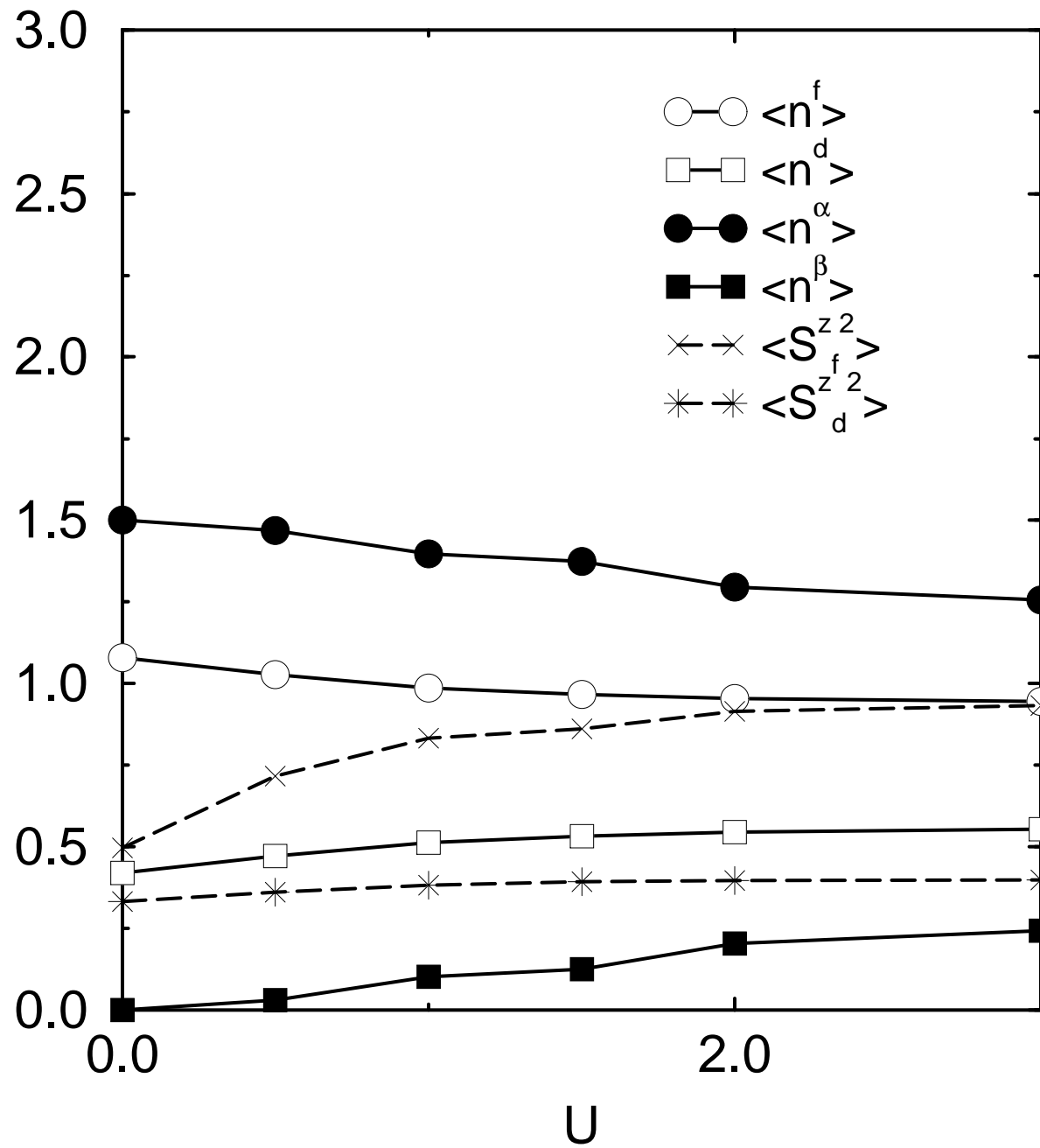


fig 12

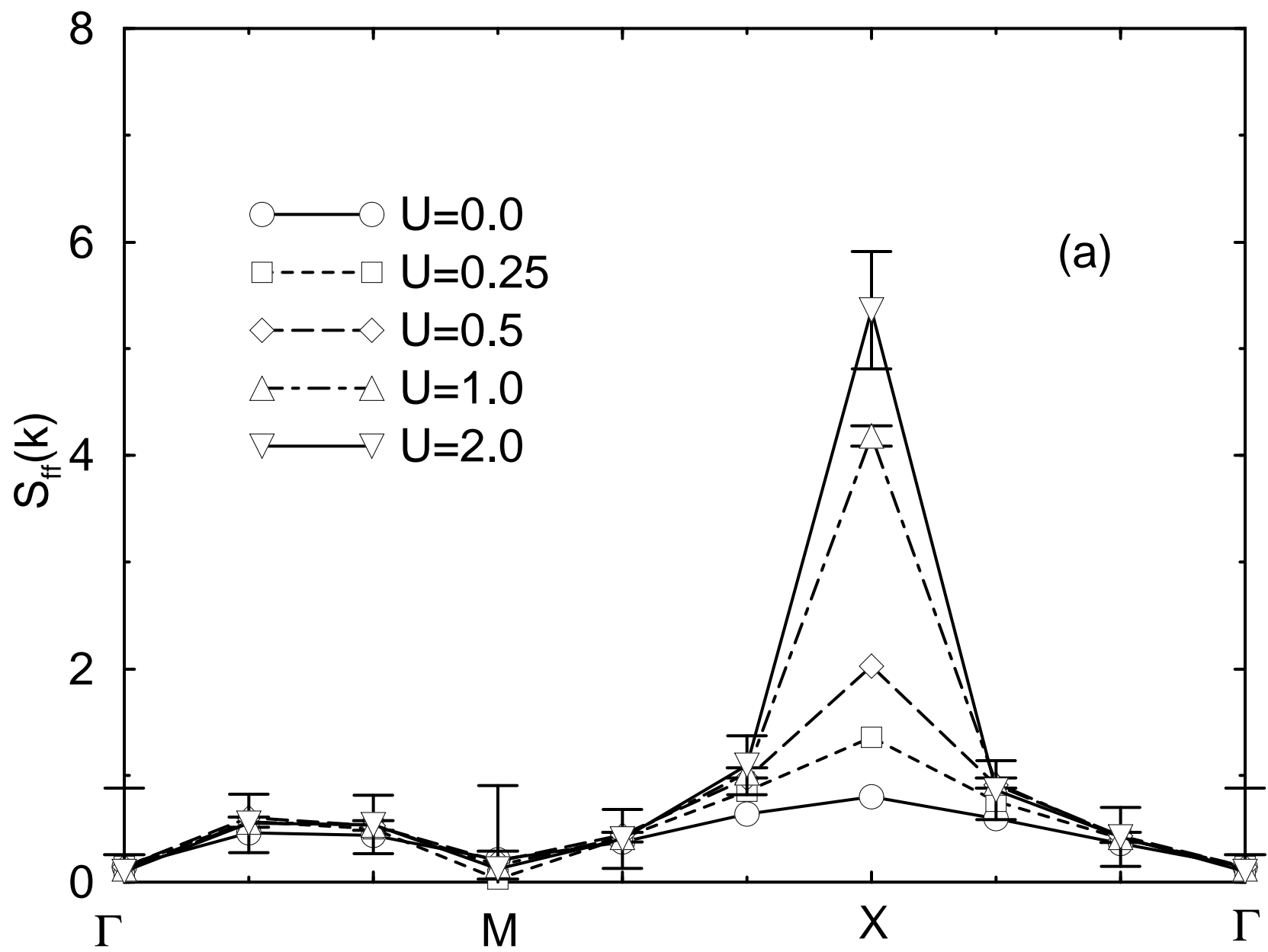


fig 13a

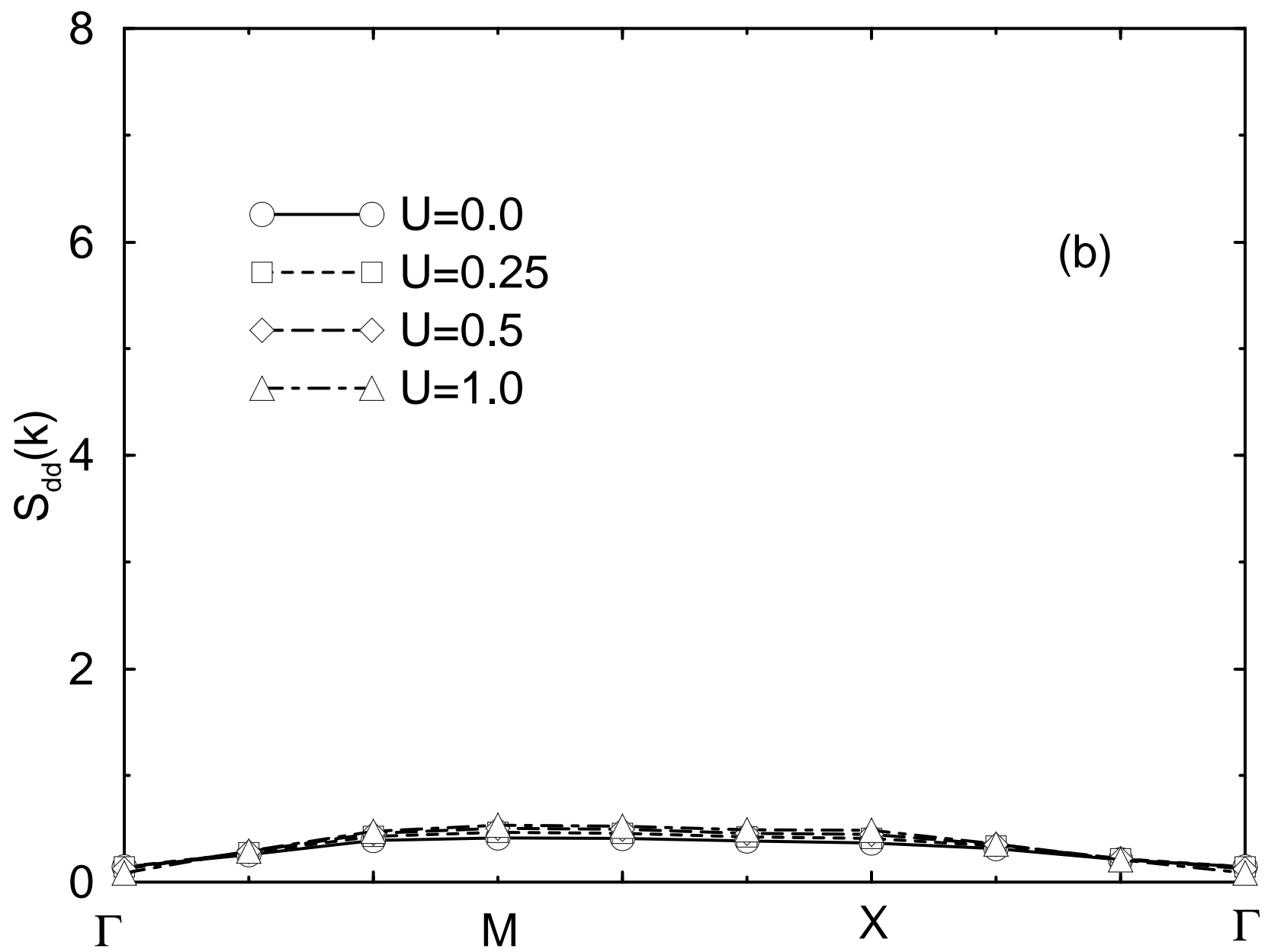


fig 13b